Deformation Index Applied to Impact

T.C. Ransom[1,2], R.M. Gamache[3], B.P. Mason[3], H.D. Ladouceur[1,*], and C.M. Roland[1]

[1]Naval Research Laboratory, Chemistry Division, Code 6105, Washington DC 20375-5342

[2]current address: Naval Surface Warfare Center, Indian Head Explosive Ordnance Disposal Technology Division, Indian Head, MD 20640

[3]Naval Postgraduate School, Department of Physics, Monterey, CA 93943-5216

[*]deceased Nov. 27, 2019

(January 22, 2020)

– Rubber Chemistry & Technology, *in press* –

ABSTRACT

Almost three decades ago, S. Futamura [*Rubber Chem. Technol.* **64**, 57 (1991).] devised the deformation index concept for determining the control parameter for the viscoelastic response of deformed elastomers. We have extended this to impact mitigation, in which typically material hardness and energy dissipation both affect the behavior. Laboratory impact tests were carried out on a series of compounds to deduce the deformation index pertinent to the rubber component. We then analyzed ballistic experiments, wherein material failure is associated with more complex conditions. The utility and limitations of this approach are discussed.

INTRODUCTION

Research and development efforts to understand collisions and ameliorate the damage from impact extend to a wide range of applications and technologies, examples including automotive collisions [1,2,3] and with the proliferation of electric automobiles, the crashworthiness of batteries [4,5]; collisions involving space debris [6,7], such as asteroids with the Earth [8]; seismic activity [9]; brain injuries due to head impact [10,11,12,13]; and military helmets [14,15,16,17,18]. The latter two are especially difficult problems because of the

complexity of the response of the brain (strain, negative and positive pressures, pressure gradients, rotation, and coup/contrecoup effects [19,20,21]) to blast or ballistic assault [22,23,24,25,26]. Collisions give rise to non-linear deformations at high strain rates that may be accompanied by both physical (cavitation, phase transitions) and chemical changes [27,28,29,30,31,32,33,34].

The starting point in mitigating the effects of impact is understanding the factors underlying damage. Modeling and simulations of impact are widely developed, spanning molecular dynamic simulations [35,36], continuum mechanics [37,38,39], and hydrocode and finite-element modeling [40,41,42,43]. In this work we adopt a simple, intuitive approach based on the deformation index concept, in which the interdependence among components is decoupled from the mechanical perturbation imposed on the system [44]. The objective is a predictive scheme that at least makes empirical test and evaluation procedures more efficient. The method has been applied to the rolling resistance of tires [44,45], heat buildup in both pneumatic [46] and nonpneumatic tires [47], and to rubber fatigue [48]. In this method a property of the system is measured and correlated with the quantity E''/E^{*n}. Here *E″* is the dynamic loss modulus, *E** the complex modulus (which for elastomers is nearly equivalent to the storage modulus), and *n* the deformation index. This correlation follows from the equation [44]

$$\mathrm{P} = k_1 E''/E^{*n} + k_2 \tag{1}$$

in which P is the property of interest and k_1 and k_2 are constants for a given system. The value of the index *n* yielding the best correlation of the measured P characterizes the nature of the

deformation. Strain-, energy-, and stress-control correspond to n = 0, 1, and 2, respectively, although non-integral values are possible for more convoluted processes.

We use the deformation index to analyze impact data, both laboratory experiments and ballistic tests. The objective is to assess the nature of the deformation experienced by the rubber component, in order to identify the properties of elastomer coatings underlying the protection afforded to armor systems subjected to impact. This has been the topic of many previous studies [49,50,51,52], with this work motivated by the fact that energy dissipation and hardness both contribute to impact protection, generally [53,54,55,56] and for armor utilizing elastomer coatings [49,57].

EXPERIMENTAL

The polymers herein were random copolymers of acrylonitrile and butadiene, NBR (Nipol from Zeon Chemical), or styrene and butadiene, SBR (Duradene from Firestone Polymers or eSBR from Lion Elastomers). Curing was effected using sulfur, 2-2'-dithiobis(benzothiazole) (MBTS), zinc oxide, and stearic acid. For the deformation index analysis to be applicable, the ratio of the storage and loss moduli cannot be constant, and the accuracy increases for greater variation of the elastic and viscous properties of the tested compounds. For this reason the dynamic moduli were varied in two ways, by incorporating reinforcing carbon black (N110 or N990) and by using polymers with different glass transition temperatures, T_g. The latter is relevant when T_g is close to the test temperature and for high strain rate experiments. The compounds are listed in Tables 1 – 4.

Isothermal dynamic mechanical measurements at various temperatures were carried out on a TA Instruments Q800 DMA in tension mode, over the frequency range $0.063 \leq \omega$ (rad/s) $\leq$

200 at a strain amplitude equal to 0.1%. Time-temperature shift factors were determined from master curves of the loss tangent, with small vertical shifts applied to superpose the storage and loss moduli [58] and obtain the viscoelastic response at higher frequencies.

For the rebound experiment, 2.5 cm diameter, 1 cm thick disks were placed on a steel base, with a cylindrical 28 g mass dropped from a fixed height of h=40 cm. Five measurements of the rebound height were made, with the sample temperature = 50 °C in order to achieve sufficient resilience in all compounds. The glass fracture test was carried out on 75×25×0.1 mm optical glass, with 25×50×2 mm rubber coatings. The test temperature was also 50 °C. A 63 g, 25 mm diameter steel sphere was used as the projectile, released from varying heights using a magnetic release. The drop height was increased incrementally until fracture was obtained. The test was repeated at this same height four times to ensure a minimum failure rate of at least 50%.

Ballistic tests at ambient temperature were carried out on a laminate of 5 mm thick rubber sheets attached to the front (strike-face) side of a 6 mm steel substrate (HHS; MIL-DTL-46100). The minimum velocity required for a 12.5 mm diameter steel projectile (MIL-DTL-46593B) to penetrate the laminate was determined, with complete penetration defined by perforation of a back-side witness plate. The test conditions complied with MIL-STD-662, with a full description found elsewhere [59].

Finite element analysis (Comsol Multiphysics®) employed a 2-D axisymmetric model of the rebound resiliometer test, with the dimensions and properties of the rubber target and steel drop weight chosen to match the experiment. The deformation index formalism utilizes frequency dependent real and imaginary moduli; for the modeling the loss was taken as the

viscosity (= $E''\tan\delta/3\omega$, where $\tan\delta$ is the loss tangent equal to the ratio of the loss and storage moduli). The extraction of the deformation index from the calculation followed the procedure in ref. [45]; to wit, the energy dissipated for each individual element was computed, the modulus increased 20%, and the model rerun to calculate the energy dissipated by that same element.

RESULTS AND DISCUSSION

REBOUND TESTS

As an initial experiment, resilience determinations were carried out for a steel projectile falling from a fixed height onto a rubber disc; a test temperature of 50 °C was chosen to give measurable rebound heights for all compounds (Table 1). Such drop tests are commonly used to characterize the dynamic behavior of materials; the square root of the rebound height relative to the drop height is known as the coefficient of restitution [60]. For these tests we calculated the Pearson linear correlation coefficient for eq. (1), with P the measured rebound of the projectile, using deformation indices in the range $0 \leq n \leq 2$. As shown in Figures 1 and 2a, the correlation of the experimental rebound data with E''/E^{*n} was greatest for n = 0.7 (R=98%). Note the analysis requires taking into account the rate-dependence of the dynamic properties. From video of the impact, we estimated the strain rate to be ca. 300 s^{-1}, which is consistent with the ratio of the impact speed (=$\sqrt{2gh}$; g=9.8 m/s^2) to rubber thickness, = 280 s^{-1}. As shown in Figure 2b, the correlation of the rebound data with E''/E^{*n} deteriorates significantly if the dynamic moduli measured at 1 s^{-1} are used, rather than the appropriate values, obtained by t-T superpositioning, at 300 s^{-1}.

Our result, n = 0.7, is in agreement with the analysis of similar rebound experiments in ref. [44]. The question that arises is why dropping a weight from a constant height does not induce constant energy deformation (n=1), corresponding to the gravitational potential in the absence of friction. To investigate this in more detail, we carried out finite element modeling of the rebound experiment. The deformation index was determined as a function of position in the rubber disk by computing the change in strain response of each element to a change in its stiffness. The results are displayed in Figure 3, where it can be seen that over most of the volume, n=1; that is, constant energy deformation, consistent with a fixed drop height. However, in the vicinity of the impact n varies strongly with position. It is this complex interaction around the point of impact that causes the net value of n to be less than unity. If the projectile cross-sectional area is significantly increased, close to that of the rubber disk, the latter now compresses uniformly (Fig. 3). This alleviates the interactions at the point of impact, and the deformation index has a net value very close to unity.

In Figure 4 is shown the compression of the rubber as a function of time after impact. The calculation was carried out for two elastomers, one having a 20% higher modulus. Interestingly, the compression of the cylinders is the same, independent of the rubber stiffness, up through roughly half the time prior to maximum penetration of the projectile. This “inertial” behavior is sensitive to the details of the finite element modeling, diminishing for a broader projectile or lower impact velocities. But at least initially the deformation is largely strain-controlled, corresponding to n = 0, and thus not dependent on the rubber properties. The significance of this becomes apparent in the glass fracture tests.

GLASS FRACTURE TESTS

To extend the deformation index method to failure, a glass/elastomer laminate was used as the target, with the drop height varied to determine the minimum necessary to fracture the (backside) glass. The compounds for this test are listed in Table 2, along with their dynamic moduli. Rate effects are important even for rigid solids [61], with frequency dependence herein obtained (using time-temperature superpositioning) at the frequency corresponding to the measured strain rate, 7.5 $\pm$ 1.5 s^{-1}. The error bars on this strain rate reflect the different drop heights required to break the glass for different coating, which of course changes the impact velocity and thus the strain rate. In Figure 5 is a plot of the minimum height to break the glass as a function of E''/E^{*n} (eq.(1) with P the drop height). The scatter in the data is larger than for the rebound tests, as expected for failure properties. The best correlation is for n = 0.35 $\pm$ 0.1. This signifies substantial strain control of the fracture process. This is in accord with the results in Fig. 4, that compression of the elastomer during the impingement phase is initially independent of the rubber modulus. The consequent flexure of the glass governs its fracture, which likely occurs prior to bottoming out and subsequent rebound of the projectile.

BALLISTIC TESTS

We extended the failure experiments to ballistic tests. A powder gun was used to propel a steel projectile at normal incidence to a rubber-coated steel target, with measurement of the minimum velocity required for penetration of the bilayer (i.e., a 50% probability of complete penetration). The rubber compounds, listed in Table 3, were comprised of polymers having different T_g, both with and without reinforcing filler. This variation ensured a range of values of the ratio of the loss and complex moduli. However, it is again necessary that the viscoelastic properties correspond to the test frequency. For ballistic tests this is ca. 10^5 s^{-1} [28], which

requires application of time-temperature superpositioning. Master curves of the dynamic moduli are shown in Figure 6, where it can be seen that ballistic impact causes the rubber response to encroach on the glass transition zone. This region of the viscoelastic spectrum is characterized by contributions from both the chain dynamics and local segmental motions. Since these have different time-temperature shift factors, time-temperature superpositioning breaks down in the transition zone [58,62]. Thus, these master curves and the obtained dynamic moduli are only approximate.

The test results are displayed in Figure 7 in the form suggested by eq. (1), with P the relative increase in the velocity of the projectile necessary to penetrate the laminate. The value of n yielding the strongest correlation is 1.3, although the scatter is substantial (R^2=0.76). The implication of n=1.3 is that ballistic penetration is mainly energy driven, but with a significant stress-control component. Since reinforcing filler increases both the energy dissipation as well as the rubber stiffness, this suggests that the filled compounds should be superior to the gum coatings, an inference borne out by the data (Figure 8). Of course, this conclusion does not require the deformation index analysis, since it is evident directly from the test results. However, the purpose of this study was to assess a potential method of circumventing, or at least making more efficient, a “make and break” empirical approach to developing better rubber ballistic coatings.

The interpretation of the data in Fig. 7 is complicated because the high strain rates associated with ballistic impact are proximate to the rubber to glass transition [28,35]. Such a viscoelastic phase change is unaccounted for by the deformation index analysis as carried out herein. The onset of this phase change is evident in images of the rubber coatings after

penetration (Figure 9 a and b). Lower T_g compounds exhibit extensive tearing, a rubbery-like response, whereas the high T_g coatings fail in a more brittle fashion with the hole produced in the rubber about the same size as the projectile. These contrasting behaviors are typical of the modes of failure of rubber coatings subjected to ballistic impact [52]. Note that the presence of reinforcing filler yields a response more like that of the higher T_g compounds (Fig. 9 c and d), which presumably contributes to their better performance.

An analysis using the deformation index has merit only if it is predictive. To assess this, we examine two polymers, polyvinylethylene and polyurea, previously found to have equivalent ballistic performance when used as coatings over steel [57]. This equivalence implies that the quantity E''/E^{*n} will be the same, using n=1.3 as determined above. (For this analysis we used shear moduli, since the rubbers were uncured.) These two materials have substantially different storage and loss moduli (Table 4), providing a stern test of the method. The deformation index quantity $G''/G^{*1.3}$ is equivalent within a few percent for the rubbers, consistent with their same ballistic performance.

DISCUSSION

There are three main assumptions inherent to applying the deformation index analysis to impact or ballistic experiments:

(i) The effects of strain and time are decoupled, allowing their separation. This enables application of a superposition integral to calculate the stress [58]

$$\sigma(t) = \int_{-\infty}^{t} E(t-\tau) f(\varepsilon) \frac{d\varepsilon(\tau)}{d\tau} d\tau \qquad (2)$$

from independent determinations of the relaxation modulus, $E(t)$, and strain function, $f(\varepsilon)$. This separability is generally valid for rubbers in the absence of strain reversal [63]. However, since eq.(1) only requires correlation of the impact response with the viscoelastic properties, the use of eq. (2) to compute the stress-stress response is unnecessary, although reliance on strain-rate separability is implicit in using low strain amplitude measurements to quantify the elastic and loss properties at strains approaching failure.

(ii) A correspondence is assumed between the dynamic and transient viscoelastic properties, analogous to the Cox-Merz rule for polymer melts [58]; that is, the characterization of the viscoelastic properties relies on dynamic mechanical characterization, which is then used to interpret the transient impact response. This assumption has been tested for various elastomers, with the conclusion that it is valid except near the glass transition zone [64].

(iii) As mentioned above, to obtain the viscoelastic moduli at the impact strain rates required invoking the time-temperature superposition principle, which is known to fail for polymers in the glass transition zone [58,62].

Since the strain rates for the rebound and glass breakage tests were not high ($<10^4$ s^{-1}), the complexities of the glass transition (items ii and iii) are not especially pertinent for these experiments. For this reason, the deformation index analysis yields a reliable description of the behavior of the rubbers in these tests. For the ballistic experiments herein, the encroachment into the glass transition zone (Fig. 6) introduces substantial error. Nevertheless, the value of the deformation index obtained for ballistic tests of the compounds in Table 3 was able to predict with surprising accuracy the ballistic performance of the two polymers in Table 4. Obviously more

general application of the method to impact tests should employ direct characterization of the viscoelastic properties at the relevant strain rates.

CONCLUSIONS

The results reported herein demonstrate the utility of the deformation index analysis. It describes simple rebound/resilience experiments, including effects due to the complex interactions at the sample interface. When applied to glass fracture, the analysis correctly accounts for the behavior during the initial compression, distinct from full penetration and recoil. And notwithstanding complications from the rubber-to-glass transition in ballistic tests, which introduces inaccuracies into the use of time-temperature superpositioning to obtain the viscoelastic properties of the rubber at the relevant strain rates, the deformation index approach was applicable to ballistic failure of rubber/metal laminates.

ACKNOWLEDGEMENTS

This work was supported by the Office of Naval Research, in part by Code 332 (R.G. Barsoum). TCR acknowledges an American Society for Engineering Education / Naval Research Laboratory postdoctoral fellowship.

REFERENCE

[1] B.J. Russo and P.T. Savolainen, A comparison of freeway median crash frequency, severity, and barrier strike outcomes by median barrier type, *Acc. Anal. Prev.* **117**, 216-224 (2018).

[2] L. Gaylor, M. Junge, and S. Abanteriba, Thoracic side airbags and structural performance in vehicle-vehicle lateral impacts, *Int. J. Crashworthiness* **23**, 108-116 (2018).

[3] A. Baroutaji, M. Sajjia, and A.-G. Olabi, On the crashworthiness performance of thin-walled energy absorbers: Recent advances and future developments, *Thin-Walled Struc.* **118**, 137-163 (2017).

[4] H. Wu, S. Kuang and H. Hou, Research on Application of Electric Vehicle Collision Based on Reliability Optimization Design Method, *Int. J. Comp. Meth.* **16**, 1950034 (2019).

[5] Z. Tao, Y. Jialin, Z. Xianglei and Z. Bing, Characteristics Numerical Research on Power Battery Impact Strength of New Energy Vehicle, *Int. J. Comp. Meth.* **16**, 1950042 (2019).

[6] D. Perna, M.A. Barucci, and M. Fulchignoni, The near-Earth objects and their potential threat to our planet, *Astron. Astrophys. Rev.* **21**, 65 (2013).

[7] J.C. Ruiz-Suarez, Penetration of projectiles into granular targets, *Rep. Prog. Phys.* **76**, 066601 (2013).

[8] Y. Qi and A. de Ruiter, Planar near-Earth asteroids in resonance with the Earth, *Icarus* **333**, 52-60 (2019).

[9] A. Kharazian and F. Lopez-Almansa, State-of-the-Art of Research on Seismic Pounding Between Buildings with Aligned Slabs, *Arch. Comp. Meth. Eng.* **26**, 327-345 (2019).

[10] K.L. Hon, A.K.C. Leung, and A.R. Torres, Concussion: A Global Perspective, *Sem. Ped. Neuro.* **30**, 117-127 (2019).

[11] A.D. Patton, A Review of Instrumented Equipment to Investigate Head Impacts in Sport, *Appl. Bionics Biomech.* 7049743 (2016).

[12] O. Duncan, et al. Review of Auxetic Materials for Sports Applications: Expanding Options in Comfort and Protection, *Appl. Sci. Basel* **8**, 941 (2018).

[13] M.F. Sonnenschein, E. Nicoli, L. Ma, and B.L. Wendt, Impact mitigation in layered polymeric structures, *Polymer* **131**, 25-33 (2017).

[14] A. Miranda-Vicario, P.M. Bravo, and F. Coghe, Experimental study of the deformation of a ballistic helmet impacted with pistol ammunition, *Comp. Struc.* **203**, 233-241 (2018).

[15] C.A. Weisenbach, K. Logsdon, R.S. Salzar, V.C. Chancey, and F. Brozoski, Preliminary Investigation of Skull Fracture Patterns Using an Impactor Representative of Helmet Back-Face Deformation, *Military Med.* **183**, 287-293 (2018).

[16] X. Yang, The Development of Military Helmet for Bare-Handed Combat, 18th International Conference on Man-Machine-Environment System Engineering, Nanjing China, Oct 2018; *Lect. Notes Elec. Eng.* **527**, 433-440 (2019).

[17] A. Haris, H.P. Lee, and V.B.C. Tan, An experimental study on shock wave mitigation capability of polyurea and shear thickening fluid based suspension pads, *Def. Tech.* **14**, 12-18 (2018).

[18] S.G. Kulkarni, X.-L. Gao, S.E. Horner, J.Q. Zheng and N.V. David, Ballistic helmets – Their design, materials, and performance against traumatic brain injury, *Comp. Struc.* **101**, 313-331 (2013).

[19] D. Marjoux, D. Baumgartner, C. Deck, and R. Willinger, Head injury prediction capability of the HIC, HIP, SIMon and ULP criteria, *Acc. Anal. Prev.* **40**, 1135-148 (2008).

[20] D. Espíndola, S. Lee, and G. Pinton, Shear shock waves are observed in the brain, *Phys. Rev. Appl.* **8**, 044024 (2017).

[21] S. Rowson and S.M. Duma, Brain Injury Prediction: Assessing the Combined Probability of Concussion Using Linear and Rotational Head Acceleration, *Ann. Biomed. Eng.* **39**, 2130 (2011); **41**, 873-882 (2013).

[22] M.L. Wilkins, Mechanics of penetration and perforation, *Int. J. Eng. Sci.* **16**, 793-807 (1978).

[23] I. Levadnyi, J. Awrejcewicz, Y. Zhang, M.F. Goethel, and Y. Gu, Finite Element Analysis of Impact for Helmeted and Non-helmeted Head, *J. Med. Biol. Eng.* **38**, 587–595 (2018).

[24] J. Sone, D. Kondziolka, J.H. Huang, and U. Samadani, Helmet efficacy against concussion and traumatic brain injury: a review, *J. Neurosurg.* **126**, 768-781 (2017).

[25] J.M. Varas, M. Philippens, S.R.Meijer, A.C. vandenBerg, P.C.Sibma, J.L.M.J. van Bree and D.V.W.M. deVries, Physics of IED blast shock tube simulations for mTBI research, *Front. Neuro.* **2**, 58 (2011).

[26] T. Rahimzadeh, E.M. Arruda, and M.D. Thouless, Design of armor for protection against blast and impact, *J. Mech. Phys. Sol.* **85**, 98-111 (2015).

[27] J.A. O'Neill, C.A. Gunnarsson, P. Moy, K.A. Masser, J.L. Lenhart, and T. Weerasooriya, Fracture Response of Cross-Linked Epoxy Resins at High Loading Rate as a Function of Glass Transition Temperature, *Dyn. Behav. Matl.* **1**, 51-58 (2017).

[28] R.B. Bogoslovov, C.M. Roland, and R.M. Gamache, Impact-induced glass transition in elastomeric coatings, *Appl. Phys. Lett.* **90**, 221910 (2007).

[29] C.M. Roland, D. Fragiadakis, R.M. Gamache, and R. Casalini, Factors Influencing the Ballistic Impact Resistance of Elastomer-Coated Metal Substrates, *Philos. Mag.* **93**, 468-477 (2013).

[30] R.A. Mrozek, B. Leighliter, C.S. Gold, Christopher, I.R. Beringer, J.H. Yu, M.R. VanLandingham, P. Moy, M.H. Foster, and J.L. Lenhart, The relationship between mechanical properties and ballistic penetration depth in a viscoelastic gel, *J. Mech. Behav. Biomed. Matl.* **44**, 109-120 (2015).

[31] E. Antillon and A. Strachan, Mesoscale simulations of shockwave energy dissipation via chemical reactions, *J. Chem. Phys.* **142**, 084108 (2015).

[32] J.A. Pathak, J.N. Twigg, K.E. Nugent, D.L. Ho, E.K. Lin, P.H. Mott, C.G. Robertson, M.K. Vukmir, T.H. Epps, and C.M. Roland, Structure Evolution in a Polyurea Segmented Block Copolymer Because of Mechanical Deformation, *Macromolecules* **41**, 7543-7548 (2008).

[33] M. Grujicic, R. Yavari, J.S. Snipes, S. Ramaswami, J. Runt, J. Tarter, and G. Dillon, Molecular-level computational investigation of shock-wave mitigation capability of polyurea, *J. Matl. Sci.* **47**, 8197-8215 (2012).

[34] Y.-C. M Wu, W.G. Hu, Y.C. Sun, D. Veysset, S.E. Kooi, K.A. Nelson, T.M. Swager, and A.J. Hsieh, Unraveling the high strain-rate dynamic stiffening in select model polyurethanes - the role of intermolecular hydrogen bonding, *Polymer* **168**, 218-227 (2019).

[35] M. Grujicic, B. Pandurangan, T. He, B.A. Cheeseman, C.-F. Yen, C.L. Randow, Computational investigation of impact energy absorption capability of polyurea coatings via deformation-induced glass transition, *Mat Sci. Eng. A* **527**, 7741-7751 (2010).

[36] V. Agrawal, G. Arya, and J. Oswald, Simultaneous Iterative Boltzmann Inversion for Coarse-Graining of Polyurea, *Macromolecules* **47**, 3378-3389 (2014).

[37] M.V. Zhikharev and S.B. Sapozhnikov, Two-scale modeling of high-velocity fragment GFRP penetration for assessment of ballistic limit, *Int. J. Impact Eng.* **101**, 42-48 (2017).

[38] H.W. Meyer and R.M. Brannon, A model for statistical variation of fracture properties in a continuum mechanics code, *Int. J. Imp. Eng.* **42**, 48-58 (2012).

[39] D.A. Shockey, Rosetta stone experiments - And a mesomechanical approach to high-strain-rate deformation and fracture, *Exp. Mech.* **47**, 581-594 (2007).

[40] P.J. Hazell, M.R. Edwards, H. Longstaff, and J. Erskine, Penetration of a glass-faced transparent elastomeric resin by a lead-antimony-cored bullet, *Int. J. Imp. Eng.* **36**, 147-153 (2009).

[41] L.H. Nguyen, T.R. Laessig, S. Shannon, W. Riedel, A.P. Mouritz, and A.C. Orifici, A methodology for hydrocode analysis of ultra-high molecular weight polyethylene composite under ballistic impact, *Comp. A – Appl. Sci. Manu*. **84**, 224-235 (2016).

[42] T. El Sayed, W. Mock, A. Mota, F. Fraternali, M. Ortiz Computational assessment of ballistic impact on a high strength structural steel/polyurea composite plate, *Comput. Mech.* **43**, 525-534 (2009).

[43] Z. Xue, J.W. Hutchinson, Neck development in metal/elastomer bilayers under dynamic stretchings, *Int. J. Sol. Struc.* **45**, 3769-3778 (2008).

[44] S. Futamura, Deformation index – Concept for Hysteretic Energy-Loss Process, *Rub. Chem. Technol.* **64**, 57-64 (1991).

[45] S. Futamura and A.A. Goldstein, Prediction And Simulation Of Tire Performance Characteristics Based On Deformation Index Concept, *Rub. Chem. Technol.* **80**, 1-21 (2016).

[46] S. Futamura and A.A. Goldstein, A simple method for handling thermomechanical coupling for temperature computation in a rolling tire, *Tire Sci. Technol.* **32**, 56-68 (2004).

[47] J.M. Gibert, B. Ananthasayanam, P.F. Joseph, T.B. Rhyne, and S.M. Cron, Deformation Index–Based Modeling of Transient, Thermo-mechanical Rolling Resistance for a Nonpneumatic Tire, *Tire Sci. Technol.* **41**, 82-108 (2013).

[48] W.V. Mars, Analysis of stiffness variations in context of strain-, stress-, and energy-controlled processes, *Rub. Chem. Technol.* **84**, 178–186 (2011).

[49] *Elastomeric Polymers with High Rate Sensitivity: Applications in Blast, Shockwave, and Penetration Mechanics*, (R.G. Barsoum, ed.) Elsevier (2015).

[50] M.R. Amini and S. Nemat-Nasser, "Micromechanisms of ductile fracturing of DH-36 steel plates under impulsive loads and influence of polyurea reinforcing," *Int. J. Fract.* **162**, 205–217 (2010).

[51] L. Xue, W. Mock, and T. Belytschko, Penetration of DH-36 steel plates with and without polyurea coating, *Mech. Matl.* **42**, 981–1003 (2010).

[52] C.M. Roland, D. Fragiadakis, and R.M. Gamache, Elastomer-steel laminate armor, *Comp. Struc.* **92**, 1059–1064 (2010).

[53] Z. Jia, Y. Yu, and L. Wang, Learning from nature: Use material architecture to break the performance tradeoffs, *Matl. & Des.* **168**, 107650 (2019).

[54] X. Xuan, Y.-R. Miao, W.L. Shaw, K.S. Suslick, and D.D. Dlott, Shock Wave Energy Absorption in Metal–Organic Framework, *J. Am. Chem. Soc.* **141**, 2220-2223 (2019).

[55] S.K. Yeh, et al., Light shear thickening fluid (STF)/Kevlar composites with improved ballistic impact strength, *J. Polym. Res.* **26**, 155 (2019).

[56] Special Issue: Glass Armor and General Glass Science, *Int. J. Appl Glass Sci.* **5**, (2015).

[57] G. Montella, C.B. Giller, A.P. Holt, D. Fragiadakis, R.M. Gamache, and C.M. Roland, Effect of temperature on the impact failure of elastomeric coatings, *J. DoD Res. & Eng.*, in press (2019).

[58] C.M. Roland, *Viscoelastic Behavior of Rubbery Materials*, Oxford Univ. Press (2011).

[59] C.M. Roland, R.M. Gamache, Measuring the blast and ballistic performance of armor, NRL Formal Report, NRL/FR/6126-15-10,284 (2015).

[60] L.J. Briggs, Methods for measuring the coefficient of restitution and the spin of a ball, J. Res. Natl. Bur. Stand. 34, 1-23 (1945).

[61] W.G. Knauss, A review of fracture in viscoelastic materials, *Int. J. Frac.* **196**, 99-146 (2015).

[62] C.M. Roland, Mechanical behavior of rubber at high strain rates, *Rubber Chem. Technol.* **79**, 429-459 (2006).

[63] P.G. Santangelo and C.M. Roland, Chain ends and the Mullins effect in rubber. *Rubber Chem. Technol.* **65**, 965-972 (1992).

[64] P.H. Mott, J.N. Twigg, C.M. Roland, K.E. Nugent, T.E. Hogan, C.G. Robertson, Comparison of the Transient Stress–Strain Response of Rubber to Its Linear Dynamic Behavior, *J. Polym. Sci. Polym. Phys. Ed.* **49**, 1194-1202 (2011).

Table 1. Rebound test (T=50 °C)

T_g	filler	E′ 300 s^{-1} (MPa)	E″ 300 s^{-1} (MPa)	rebound (%)
-20 °C	0†	3.2	0.47	61.8±0.1
		3.4	0.45	61.8±0.1
		3.5	0.52	64.2±0.3
	40 phr N990	6.1	0.90	58.2±0.1
	20 phr N110	7.9	1.2	54.7±0.3
	30 phr N110	15.5	2.5	48.6±0.2
	40 phr N110	23.7	4.0	44.3±0.05
0 °C	0	5.3	2.2	30.3±0.3
	40 phr N990	12.4	5.0	28.8±1
	20 phr N110	18.3	7.1	24.6±0.1
	30 phr N110	34.7	12.2	22.0±0.1
	40 phr N110	52.9	16.6	20.8±0.8

† varying crosslink density

Table 2. Glass breakage test (T=50 °C)

T_g	filler	E′ 7.5×10^3 s^{-1} (MPa)	E″ 7.5×10^3 s^{-1} (MPa)	glass break height (cm)
-20 °C	0†	4.6	1.9	536±50
		4.4	2.2	536±50
		5.3	3.4	536±50
	40 phr N990	8.6	4.3	572±50
	20 phr N110	11	5.1	866±100
	30 phr N110	24	19.1	866±100
	40 phr N110	36	15.2	866±100
0 °C	0	14.3	16.2	899±50
	40 phr N990	32.2	34	932±50
	20 phr N110	46.2	40	988±50
	30 phr N110	81	57	1,210±75
	40 phr N110	106	62	1,210±75

† varying crosslink density

Table 3. Ballistic test (n=1.3)

sample	T_g (°C)	N110 filler (phr)	E' 10^5 s^{-1} (MPa)	E" 10^5 s^{-1} (MPa)	E"/E*^{n}	increase in penetration velocity (%)
SBR-1g	-27	0	48	77	0.219	40.9
SBR-1f		40	155	138	0.134	42.2
SBR-2g	-42	0	22	27.4	0.268	46.4
SBR-2f		40	105	73	0.133	45.2
SBR-3g	-55	0	10.6	11.3	0.321	38.6
SBR-3f		40	69.	44.	0.143	46.4
SBR-4g	-70	0	4.9	2.1	0.238	40.1
SBR-4f		40	52.	15.	0.084	47.5

Table 4. Application of deformation index to ballistic data

polymer	T_g (°C)	G' 10^5 s^{-1} (MPa)	G" 10^5 s^{-1} (MPa)	G"/(G*$^{1.3}$)
polyvinylethylene	-0.6	242	36.9	0.029
polyurea	-64.9	83.0	8.9	0.028

Figure Captions

Figure 1. Goodness-of-fit of E''/E^{*n} for rebound data, with the best correlation achieved for n=0.7

Figure 2. Rebound measured for the coatings in Table 1 versus the deformation index variable with n = 0.7 and dynamic properties at (a) 300 and (b) 0.1 s^{-1}. Coefficient of determination is indicated.

Figure 3. Finite-element calculations of the deformation index as a function of position for (left) projectile tip similar to that used experimentally; (right) a flat projectile that more uniformly compresses the rubber disk. The scale bar spans the range of deformation indices from stress-control (n=2) to strain-control (n=0).

Figure 4. Finite element calculation of the penetration of the projectile for rubber disks having storage and loss moduli that differ by a factor of 1.2. Note the effect of rubber modulus becomes apparent only after the first 150 μs.

Figure 5. Minimum drop height to break glass having the rubber coatings in Table 2 versus the deformation index parameter with n=0.35. Inset shows the fit quality as a function of n, with the maximum at n=0.35±0.1.

Figure 6. Dynamic mechanical master curves at a reference temperature of 25 °C for the elastomers in Table 3: (top) unfilled; (bottom) carbon-black reinforced. The horizontal dotted line denotes the approximate frequency of the ballistic test. With increasing glass transition temperature of the coating, the impact occurs further into the glass transition zone.

Figure 7. Relative increase in the minimum projectile velocity for complete penetration of the rubber/steel laminate for the compounds listed in Table 3. Deformation index best describing the data, n=1.3, has a Pearson's correlation coefficient of 87%.

Figure 8. Comparison of the relative increase in penetration velocity for targets having coatings with and without reinforcing carbon black.

Figure 9. Front face of targets after ballistic test: (a) SBR-4g, gum rubber, T_g=–70°C; (b) SBR-1g, gum rubber, T_g =–27°C; (c) SBR-3g, gum rubber, T_g =–55°C; (d) SBR-3f, filled rubber, T_g =–55°C.

Figure 1.

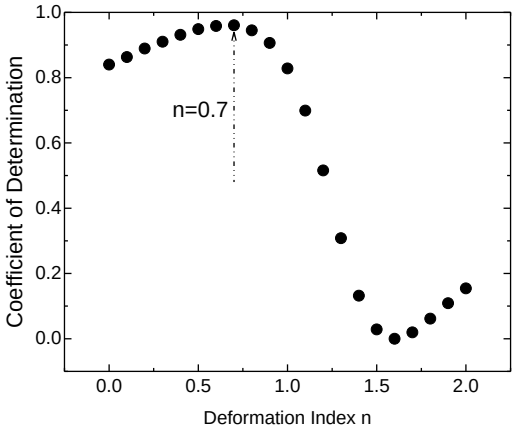

Figure 2.

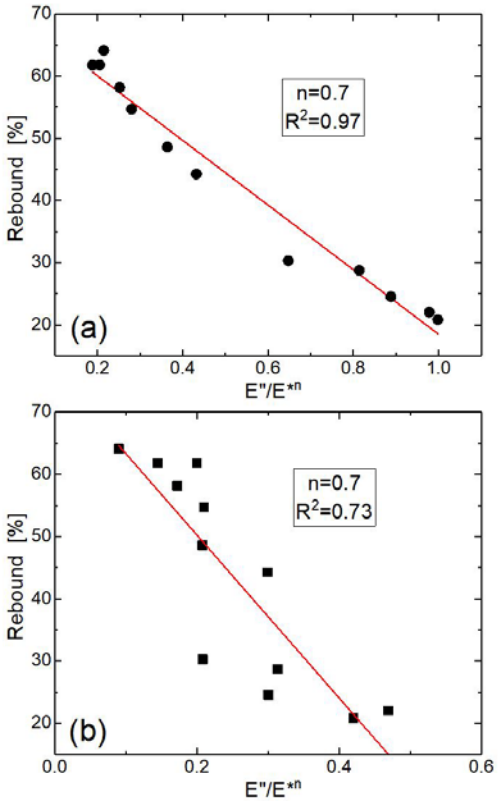

Figure 3.

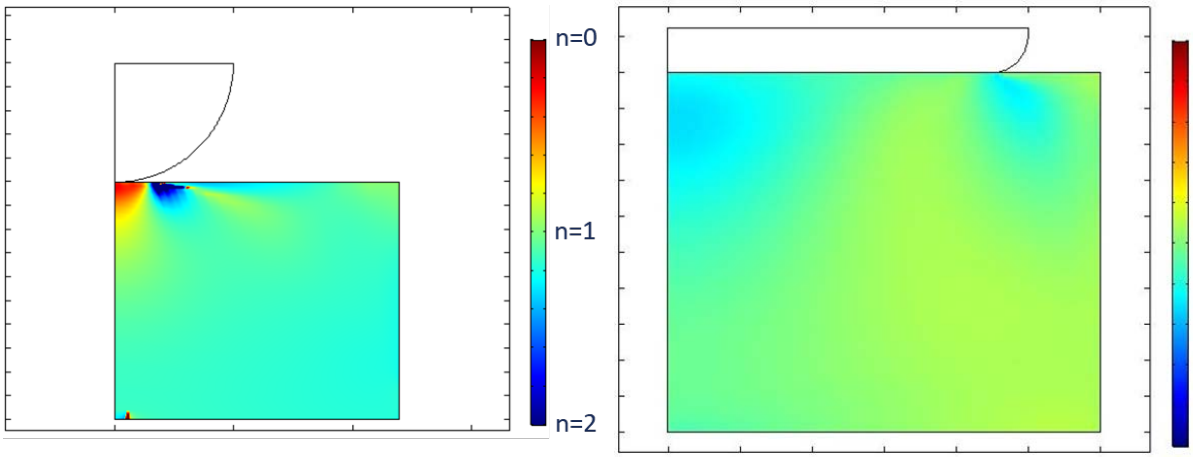

Figure 4.

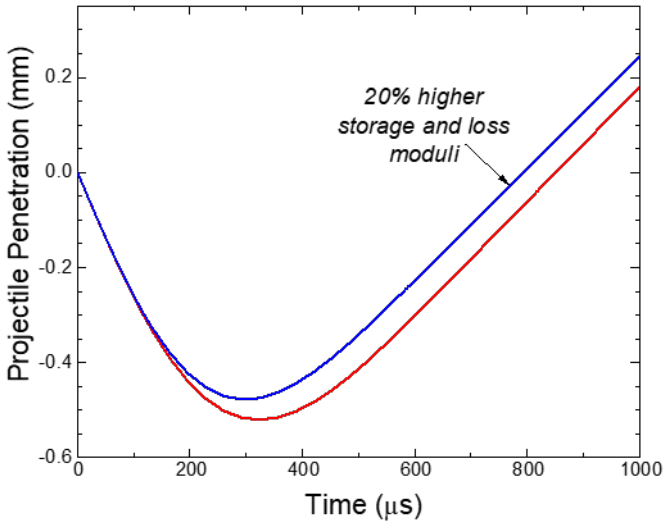

Figure 5.

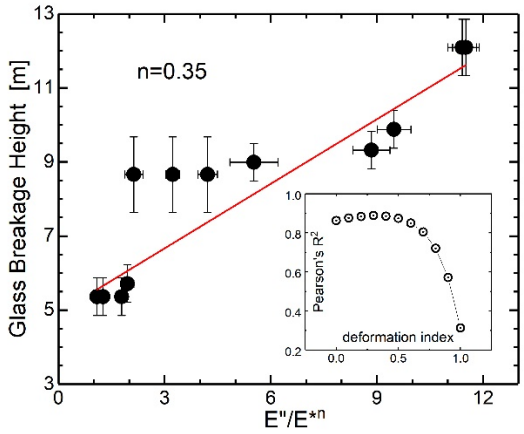

Figure 6.

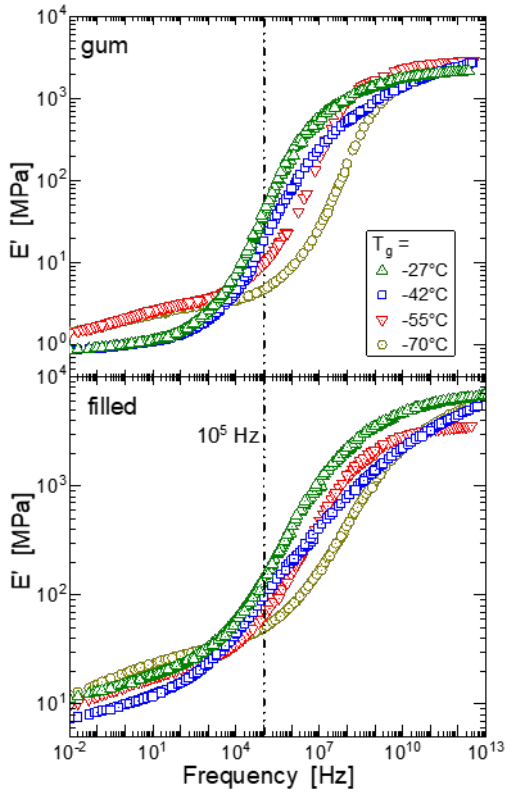

Figure 7.

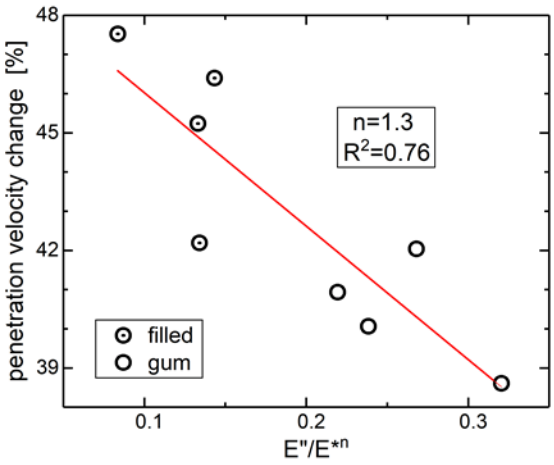

Figure 8.

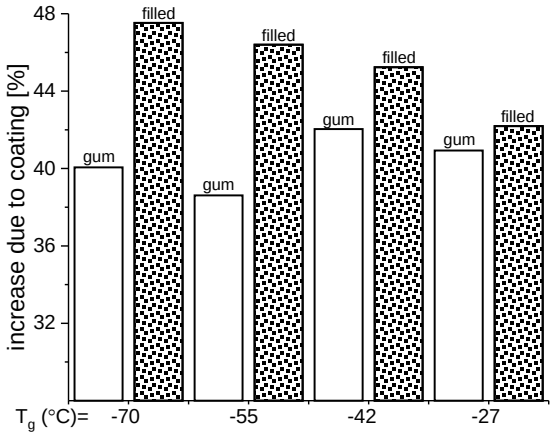

Figure 9.